Developing Modular Reflective EM Skins to Boost Wireless Signals in Cities

P. Rocca, P. Da Rù, N. Anselmi, M. Salucci, G. Oliveri, and A. Massa

2024/07/12

Contents

1 Simple Layout Scenario Validation

To gather an understanding of the correct functioning of the system a simple scenario was defined, composed by two roads meeting orthogonally, with a transmitting base station at one end and a blind region on the other end. The smart skin was deployed at the meeting point on the wall directly facing the base station, so that the power loss related to the direction of the impinging wave was minimized. A possible representation of this scenario is proposed in the following Figure 1, to better visualize the condition in which the system was tested. It's important to notice how the building facade of Figure 1(*b*) offers an ample empty space on which it is possible to accomodate a smart skin built on a very simple layout, such as the one considered in this Section.

For this scenario the considered spatial parameters and coordinates fully match the ones of the previous analysis on the surface's influence.

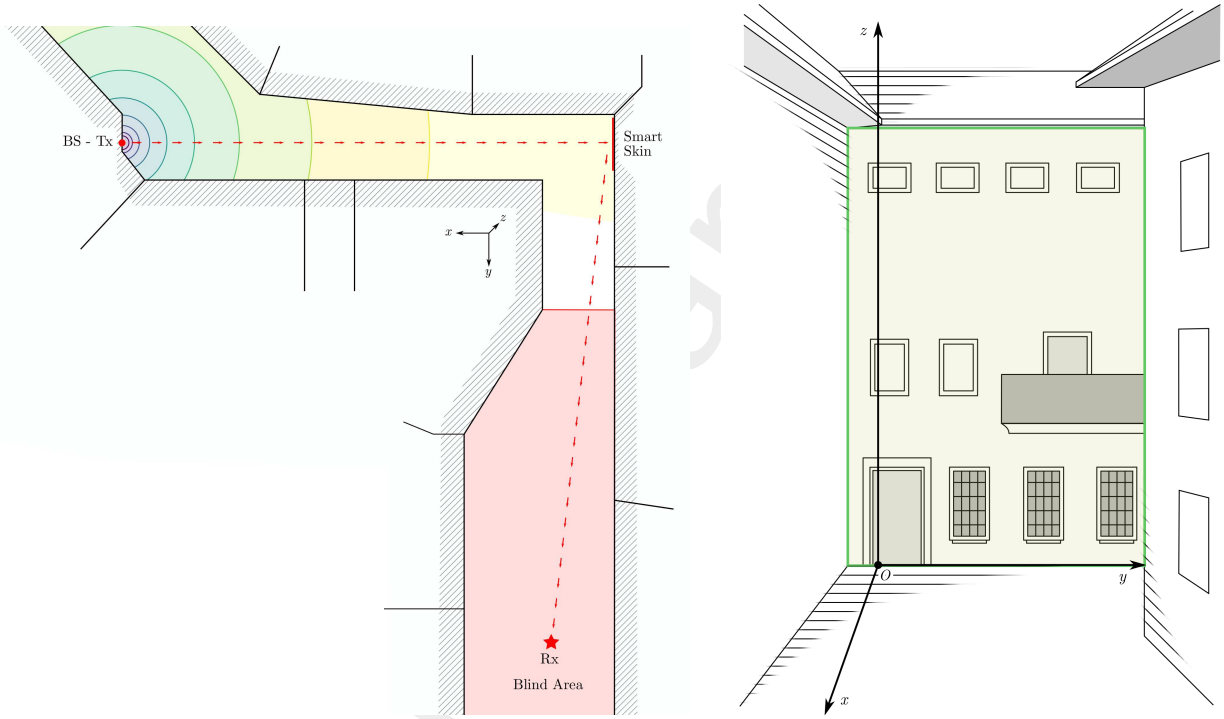

(*a*) Top-down representation of the communication scenario

(*b*) Hypothetical site for an EM smart skin urban deployment

Figure 1: Communication scenario conceptualization considered for the early validation of the software - the green rectangle on the building facade denotes the area available for the metasurface's positioning

For this early validation, three series of simulations have been performed, considering increasingly larger deployments (total number of surfaces $N_{tot} = 10$, 30 and 60), for which both the focused and the distributed radiation regime for the EM smart skin have been simulated.

To validate the results on a statistical level, each simulation has been repeated ten times with different random seeds, all leading to similar solutions, so no relevant differences between the results need to be reported.

1.1 Considerations on observer positions

The choice of the observer points, i.e., the M points in which the electric field fould be evaluated in the computation, has been the subject of a brief analysis, to evaluate its impact on the final optimization process, as reported in Figure 2. The first case considered consists in just a single observer, on the central point of the AoI ($\underline{r} = [5, 200, 1.5]$) - Figure 2($a$). This case is too simplistic and it fails to account for the variations in the field caused by the distribution of the radiation points. The second case considers five observers, with two placed on the very limit of the AoI, as in Figure 2(b). This case offers a more distributed evaluation of the field, but the closeness with the edge of the AoI could result in tainted or less robust results. The choice was then to have nine observers scattered in the AoI uniformly as in Figure 2(c). This accounts for the more fragile zones of the blind area (the corners, for the case of the focused smart skin), while maintaining all the evaluations inside it, thus keeping the results valid. A further test was done creating a grid of 21×101 observer points, for a total of $M = 2121$ observers, over which the field was optimized.

A rough comparison between the obtained results in the four cases is reported in Figure 3, from which it emerges how the difference between the cases tends to be limited, with the case considering the single central observer distancing itself the most from the general behaviour. Since these differences were not considered to be relevant for the scope of the activity, while the computational time for larger amount of observers was profoundly increased, the case with $M = 9$ was chosen for all the considered simulations. Future developments could very well further analyze this aspect, to possibly provide different and more interesting testing conditions for the final optimization.

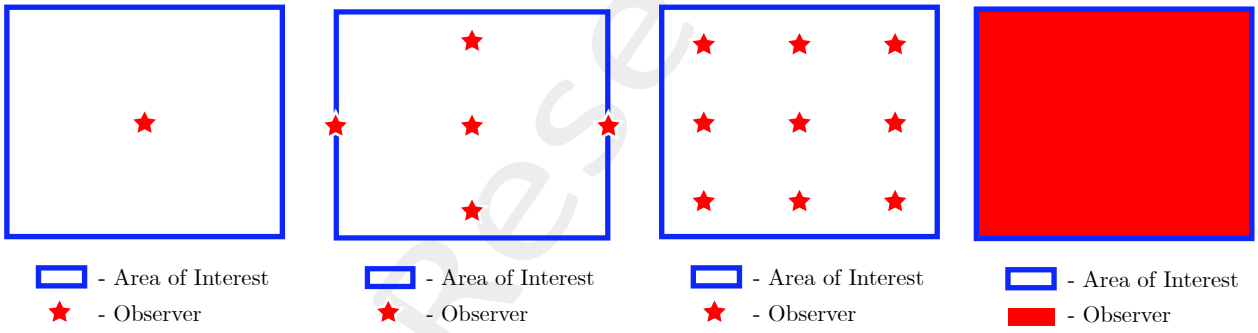

(a) $M = 1$ observer (b) $M = 5$ observers (c) $M = 9$ observers (d) $M = 2121$ observers

Figure 2: Considered observer positions in the AoI

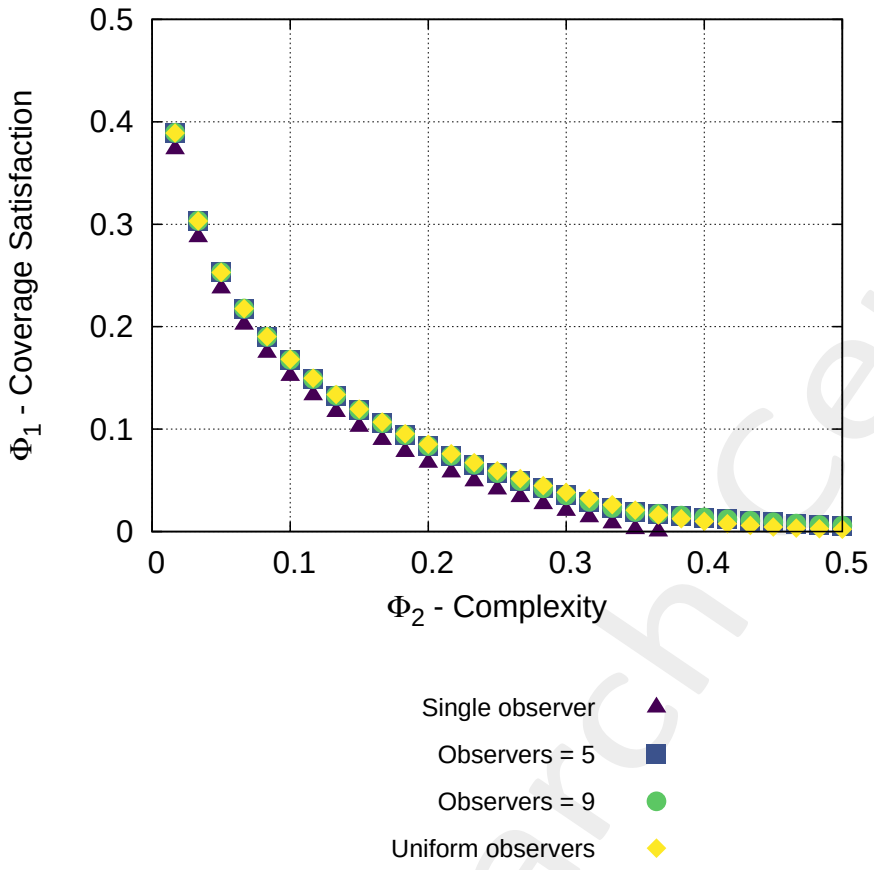

Figure 3: Comparison of Pareto fronts achieved by the four considered scenarios

The coordinates of the observer points for the chosen distribution [Figure 2 (*c*)] are reported in Table I.

Table I: Observer coordinates for the smart skin optimization

#	x [m]	y [m]	#	x [m]	y [m]	#	x [m]	y [m]
1	2.5	180	4	5	180	7	7.5	180
2	2.5	200	5	5	200	8	7.5	200
3	2.5	220	6	5	220	9	7.5	220

1.2 N = 10 metasurfaces

The first couple of simulations have been performed considering a smart skin composed of just 10 metasurfaces, arranged on two rows and five columns. The coordinates of the centers of these surfaces and a schematic visualization are reported in Table II and Figure 4.

Table II: Coordinates of the metasurfaces that compose the smart skin in the case for N = 10. Surfaces are square, with side of 0.5 [m].

#	y_{center} [m]	z_{center} [m]	#	y_{center} [m]	z_{center} [m]
1	0	8	**6**	0	7.5
2	0.5	8	**7**	0.5	7.5
3	1	8	**8**	1	7.5
4	1.5	8	**9**	1.5	7.5
5	2	8	**10**	2	7.5

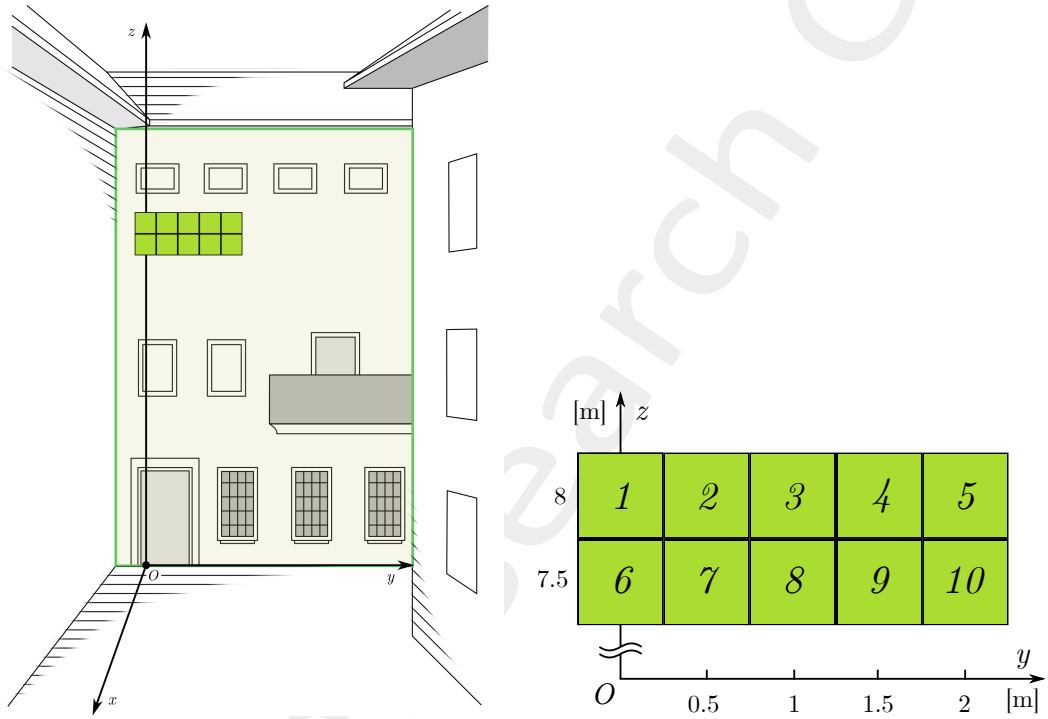

(*a*) Smart skin deployment on building facade (*b*) Metasurfaces' position and ID

Figure 4: Early considered smart skin deployment for N=10 metasurfaces

1.2.1 Focused smart skin radiation

The term "focused smart skin radiation" refers to the configuration presented, in which all the metasurfaces that compose the smart skin are set to radiate the incoming signal towards the center of the area of interest - $\underline{r} = [5, 200, 1.5]$.

The result of this optimization cycle presents the Pareto front of Figure 5, where the behaviour is akin to the expected one, with a well defined Pareto front and all the solutions of the previous iterations contained by it. Figure 6 reports the field results and smart skin configuration for one of optimal solutions on the Pareto front.

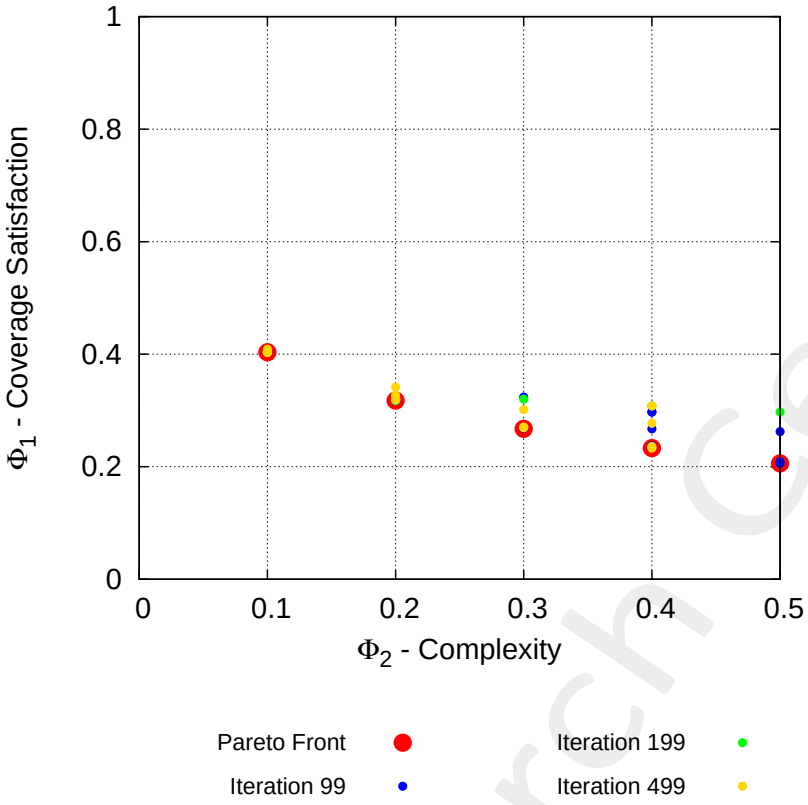

Figure 5: Optimization results (Pareto front in red)

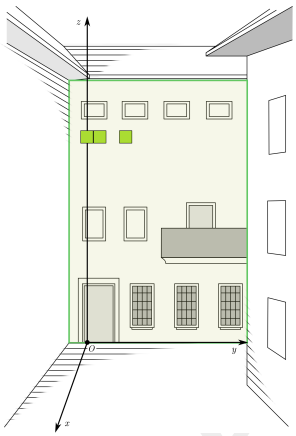

(*a*) Smart skin configuration

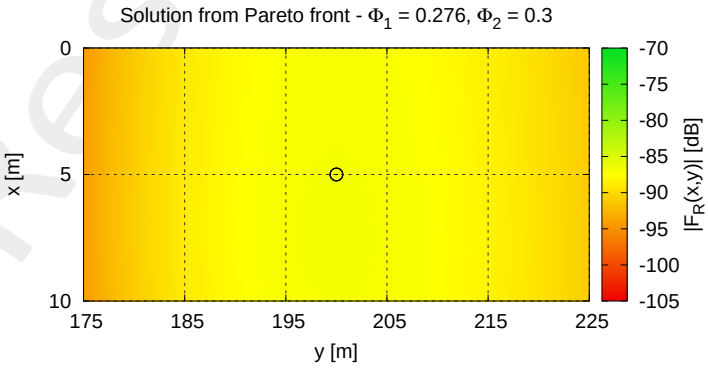

(*b*) Field inside the AoI

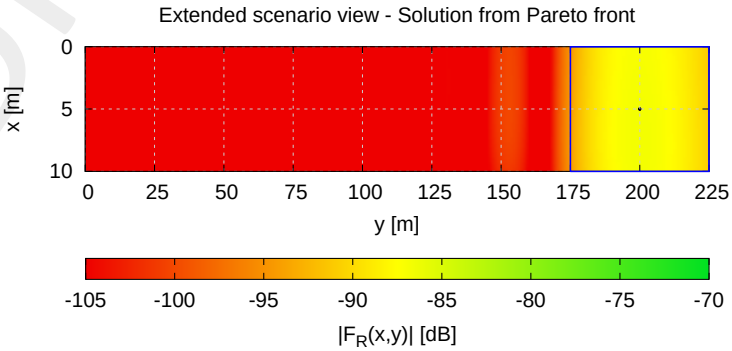

(*c*) Extended scenario view - AoI in blue

Figure 6: Solution ID 80 - $\Phi_1 = 0.276$, $\Phi_2 = 0.3$

1.2.2 Distributed smart skin radiation

The "distributed smart skin radiation" scenario involves, as explained, a smart skin whose composing metasurfaces radiate each one towards a single point inside the AoI, which are generally distributed in a uniform manner. The coordinates for the radiation points for 10 metasurfaces are reported in the following Table III.

Table III: Radiation points (x, y) coordinates for the distributed radiation of the smart skin for N = 10 metasurfaces

Surface ID	x [m]	y [m]	Surface ID	x [m]	y [m]
1	2.5	180	**6**	7.5	180
2	2.5	190	**7**	7.5	190
3	2.5	200	**8**	7.5	200
4	2.5	210	**9**	7.5	210
5	2.5	220	**10**	7.5	220

Once again, the Pareto front is formed correctly, as reported in Figure 7, and one of its solutions is further developed in Figure 8, with a representation of the smart skin and its corresponding field.

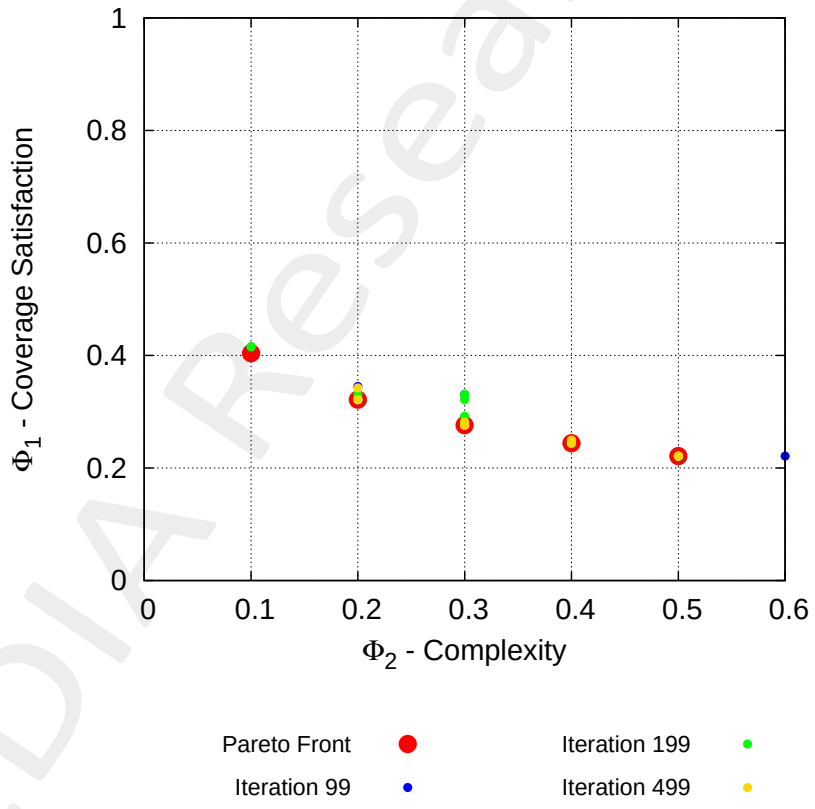

Figure 7: Optimization results (Pareto front in red)

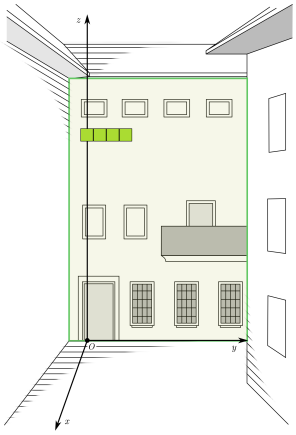

(*a*) Smart skin configuration

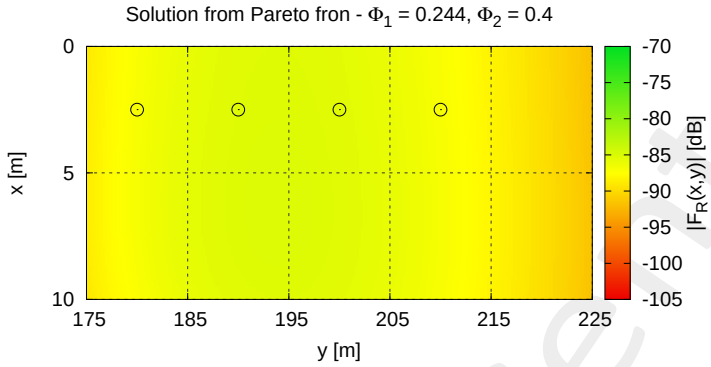

(*b*) Field inside the AoI

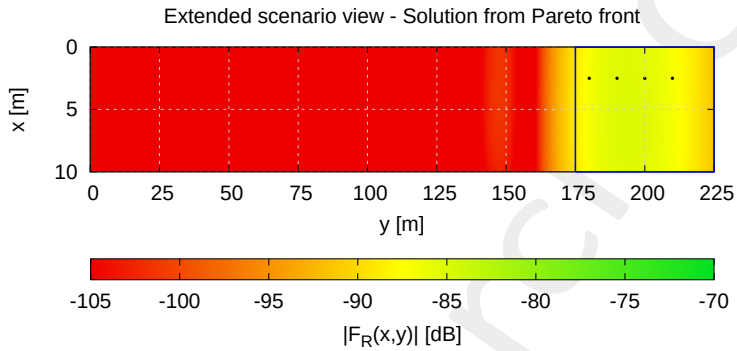

(*c*) Extended scenario view - AoI in blue

Figure 8: Solution ID 158 - $\Phi_1 = 0.244$, $\Phi_2 = 0.4$

1.2.3 Considerations and comments

From a comparison of the data resulting from the two iterations of the optimization of the smart skin composed of N = 10 metasurfaces, presented in the following Figure 9, it is possible to see how the two obtained Pareto fronts differ by a small margin, with the case of focused radiation achieving slightly better field values for equal percentages of present surfaces, plausibly thanks to the higher average field value resulting from the analysis proposed.

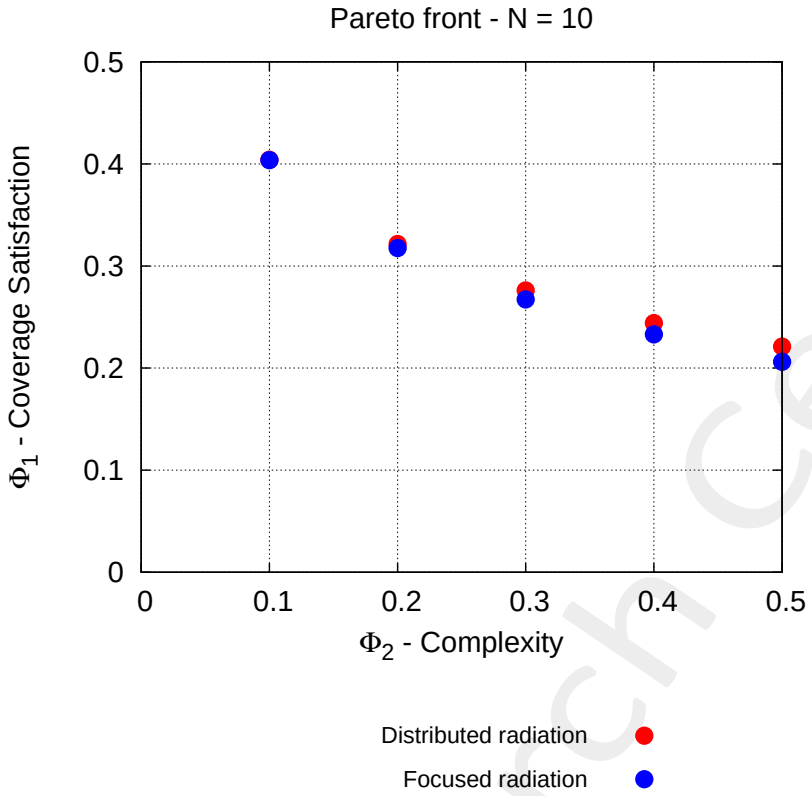

Figure 9: Comparison of focused and distributed radiation results fo N = 10

1.3 N = 30 metasurfaces

Additional simulation cycles have been conducted for the case in which N = 30 maximum metasurface positions were available on the building facade. The surfaces were arranged on a 5×6 grid, and their coordinates are reported in the following Table IV, while their representation is offered in Figure 10.

Table IV: Coordinates of the metasurfaces that compose the smart skin in the case for N = 30. Surfaces are square, with side of 0.5 [m].

#	y_{center} [m]	z_{center} [m]	#	y_{center} [m]	z_{center} [m]	#	y_{center} [m]	z_{center} [m]
1	0	8	**11**	2	7.5	**21**	1	6.5
2	0.5	8	**12**	2.5	7.5	**22**	1.5	6.5
3	1	8	**13**	0	7	**23**	2	6.5
4	1.5	8	**14**	0.5	7	**24**	2.5	6.5
5	2	8	**15**	1	7	**25**	0	6
6	2.5	8	**16**	1.5	7	**26**	0.5	6
7	0	7.5	**17**	2	7	**27**	1	6
8	0.5	7.5	**18**	2.5	7	**28**	1.5	6
9	1	7.5	**19**	0	6.5	**29**	2	6
10	1.5	7.5	**20**	0.5	6.5	**30**	2.5	6

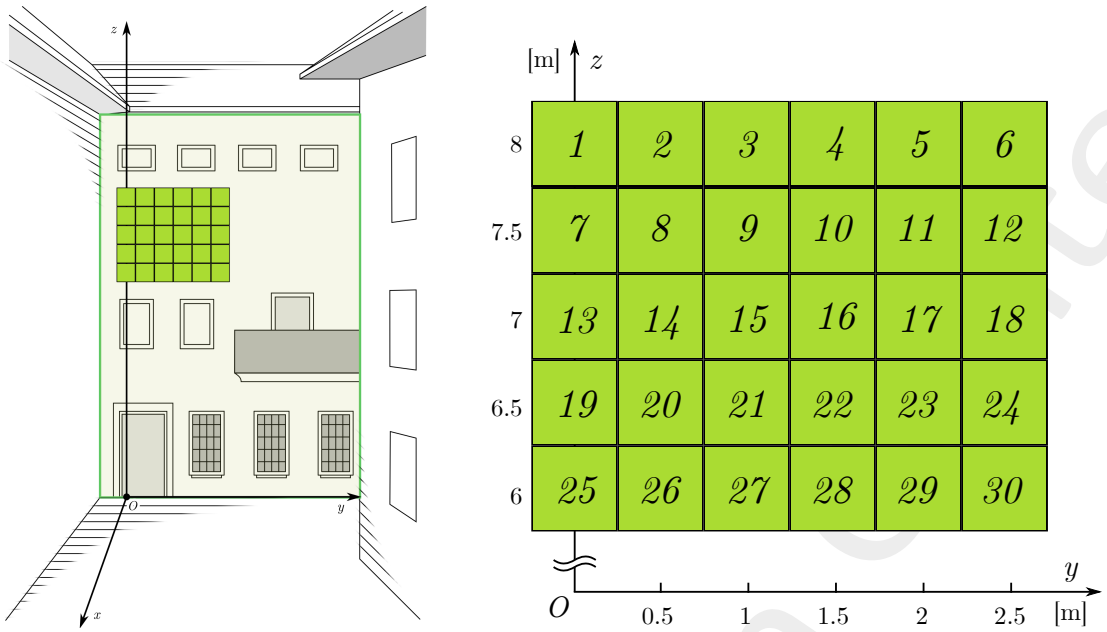

(*a*) Smart skin deployment on building facade (*b*) Metasurfaces' position and ID

Figure 10: Early considered smart skin deployment for N=30 metasurfaces

1.3.1 Focused smart skin radiation

The result for the focused smart skin are hereby presented, in the form of the obtained Pareto front (Figure 11) and one of its solutions more thorougly analyzed (Figure 12).

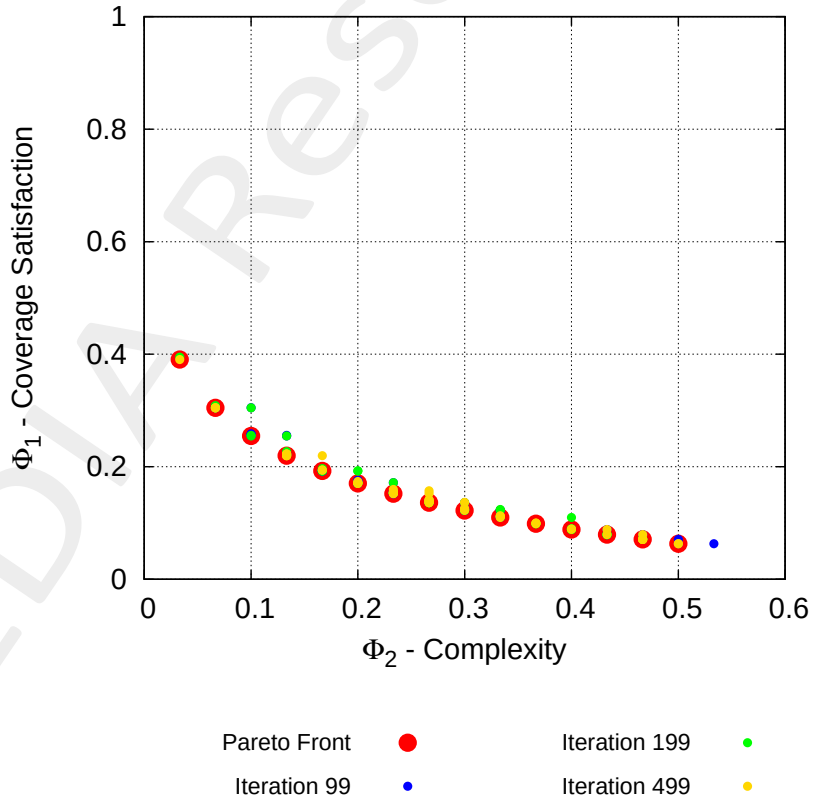

Figure 11: Optimization results (Pareto front in red)

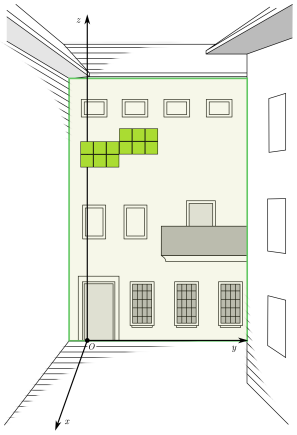

(*a*) Smart skin configuration

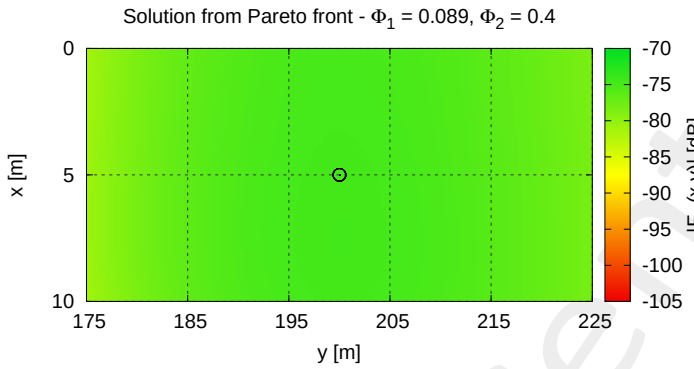

(*b*) Field inside the AoI

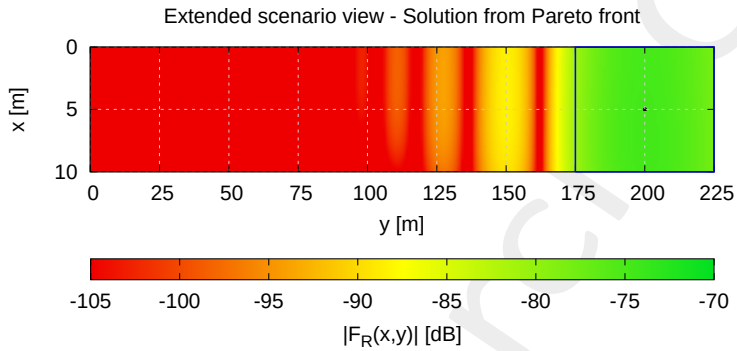

(*c*) Extended scenario view - AoI in blue

Figure 12: Solution ID 1334 - $\Phi_1 = 0.089$, $\Phi_2 = 0.4$

1.3.2 Distributed smart skin radiation

For the distributed radiation in the case of $N = 30$ metasurfaces a set of 30 radiation points have been defined. These points try to uniformly cover the metasurface, maintaining the same underlying logic of the distributed radiation in the previous $N = 10$ case. Their coordinates are reported in Table V, while the obtained results are resumed in Figures 13 and 14.

Table V: Radiation points (x, y) coordinates for the distributed radiation of the smart skin for N = 30 metasurfaces

Surface ID	**x [m]**	**y [m]**	**Surface ID**	**x [m]**	**y [m]**	**Surface ID**	**x [m]**	**y [m]**
1	2	182	**11**	5	182	**21**	8	182
2	2	186	**12**	5	186	**22**	8	186
3	2	190	**13**	5	190	**23**	8	190
4	2	194	**14**	5	194	**24**	8	194
5	2	198	**15**	5	198	**25**	8	198
6	2	202	**16**	5	202	**26**	8	202
7	2	206	**17**	5	206	**27**	8	206
8	2	210	**18**	5	210	**28**	8	210
9	2	214	**19**	5	214	**29**	8	214
10	2	218	**20**	5	218	**30**	8	218

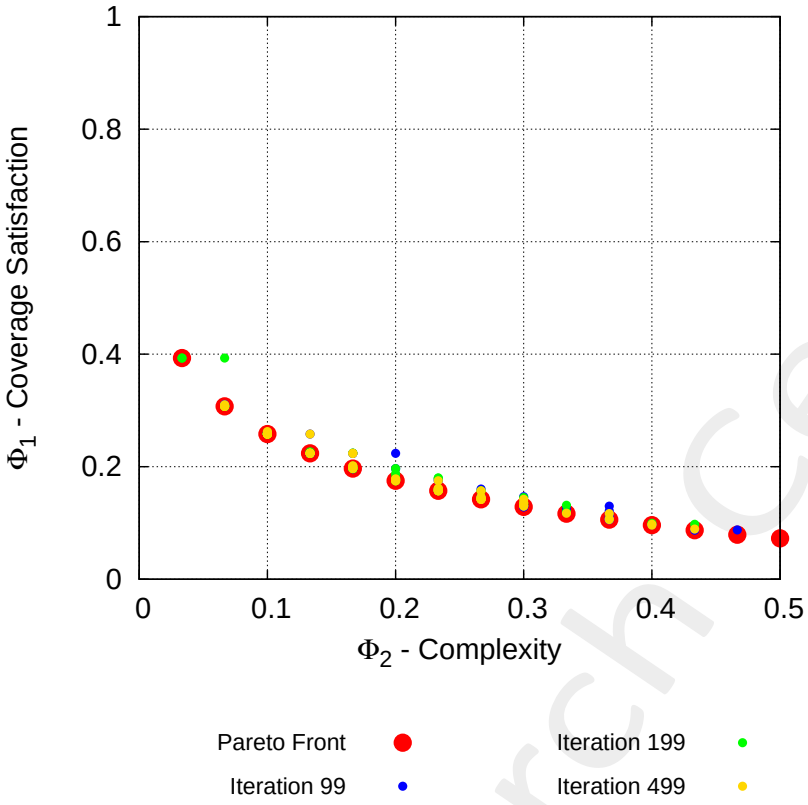

Figure 13: Optimization results (Pareto front in red)

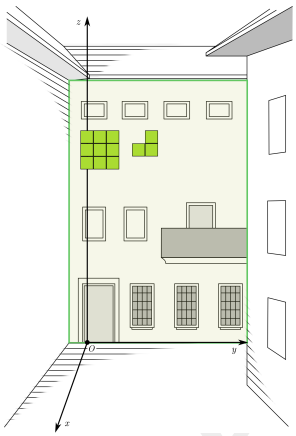

(*a*) Smart skin configuration

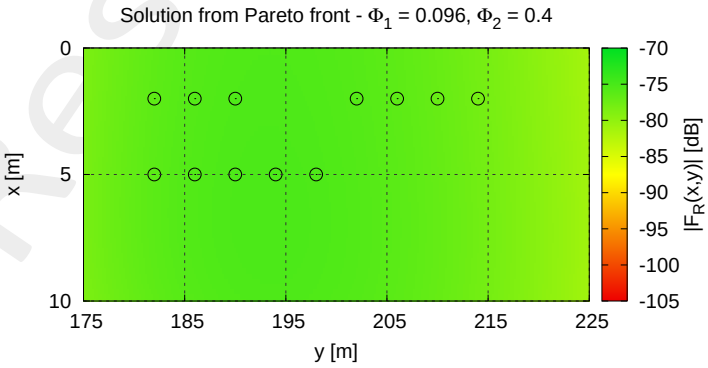

(*b*) Field inside the AoI

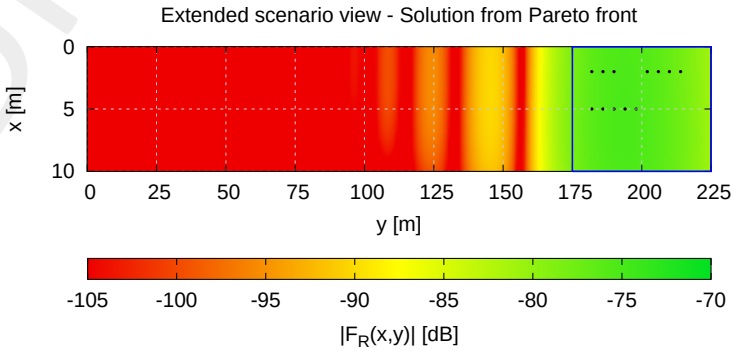

(*c*) Extended scenario view - AoI in blue

Figure 14: Solution ID 1375 - $\Phi_1 = 0.096$, $\Phi_2 = 0.4$

1.3.3 Considerations and comments

Once again, a comparison of the obtained data from the optimization of the smart skin composed of N = 30 metasurfaces, it is clear - Figure 15 - that the two Pareto fronts match almost perfectly, with the case of focused radiation achieving slightly better field values due to the better average performance analyzed.

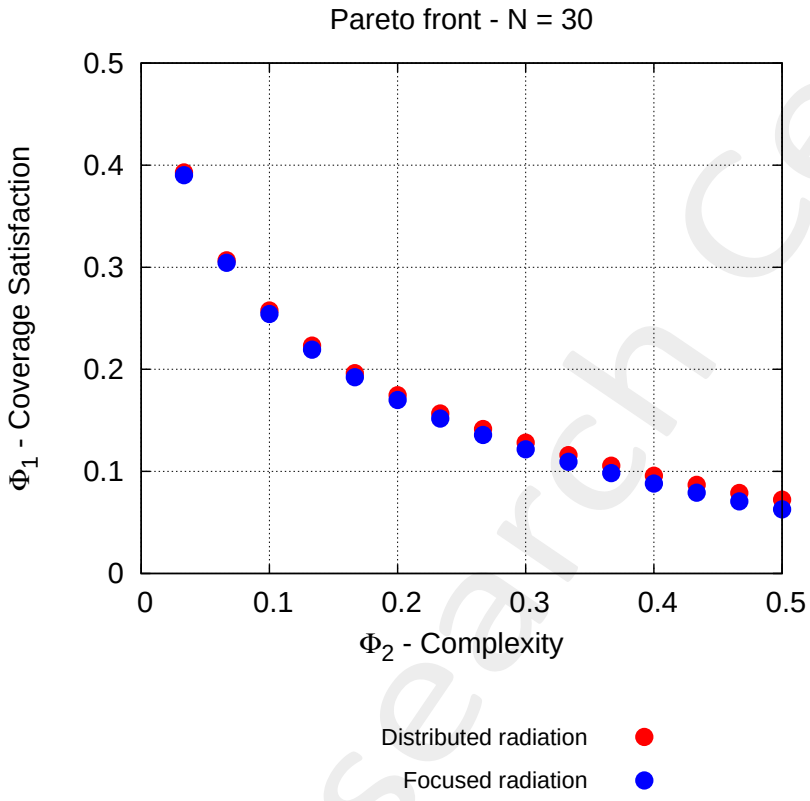

Figure 15: Comparison of focused and distributed radiation results fo N = 30

1.4 N = 60 metasurfaces

The final series of simulations considered the largest smart skin deployment, composed of N = 60 maximum metasurfaces, arranged according to the coordinates in Table VI, as in Figure 16.

Table VI: Coordinates of the metasurfaces that compose the smart skin in the case for N = 60. Surfaces are square, with side of 0.5 [m].

#	y_{center} [m]	z_{center} [m]	#	y_{center} [m]	z_{center} [m]	#	y_{center} [m]	z_{center} [m]
1	0	8	**21**	1	6.5	**41**	5	7.5
2	0.5	8	**22**	1.5	6.5	**42**	5.5	7.5
3	1	8	**23**	2	6.5	**43**	3	7
4	1.5	8	**24**	2.5	6.5	**44**	3.5	7
5	2	8	**25**	0	6	**45**	4	7
6	2.5	8	**26**	0.5	6	**46**	4.5	7
7	0	7.5	**27**	1	6	**47**	5	7
8	0.5	7.5	**28**	1.5	6	**48**	5.5	7
9	1	7.5	**29**	2	6	**49**	3	6.5
10	1.5	7.5	**30**	2.5	6	**50**	3.5	6.5
11	2	7.5	**31**	3	8	**51**	4	6.5
12	2.5	7.5	**32**	3.5	8	**52**	4.5	6.5
13	0	7	**33**	4	8	**53**	5	6.5
14	0.5	7	**34**	4.5	8	**54**	5.5	6.5
15	1	7	**35**	5	8	**55**	3	6
16	1.5	7	**36**	5.5	8	**56**	3.5	6
17	2	7	**37**	3	7.5	**57**	4	6
18	2.5	7	**38**	3.5	7.5	**58**	4.5	6
19	0	6.5	**39**	4	7.5	**59**	5	6
20	0.5	6.5	**40**	4.5	7.5	**60**	5.5	6

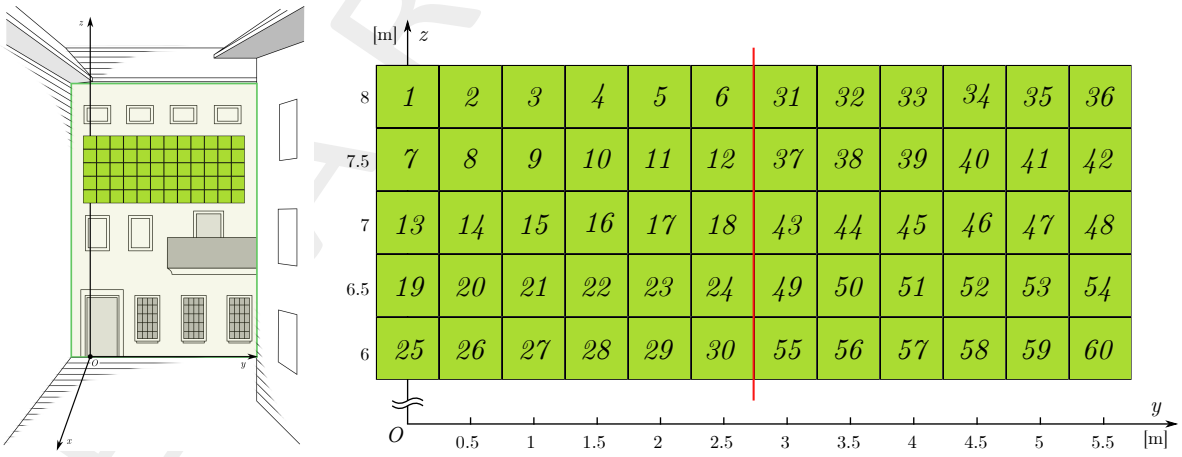

(*a*) Smart skin deployment (*b*) Metasurfaces' position and ID

Figure 16: Early considered smart skin deployment for N=60 metasurfaces

1.4.1 Focused smart skin radiation

In this test case, analogously to the previous sections, all 60 metasurfaces were set to point towards a single point, i.e., the center of the AoI - $\underline{r} = [5, 200, 1.5]$. In Figure 17 the resulting Pareto front, with one specific solution analyzed in Figure 18. It is interesting to notice how the case for N = 60 is the only one to achieve a value of 0 on the cost function ϕ_1, which means that is the fist case in which the optimization algorithm is able to obtain a configuration in which all the considered observers are above the required threshold of -70 [dB].

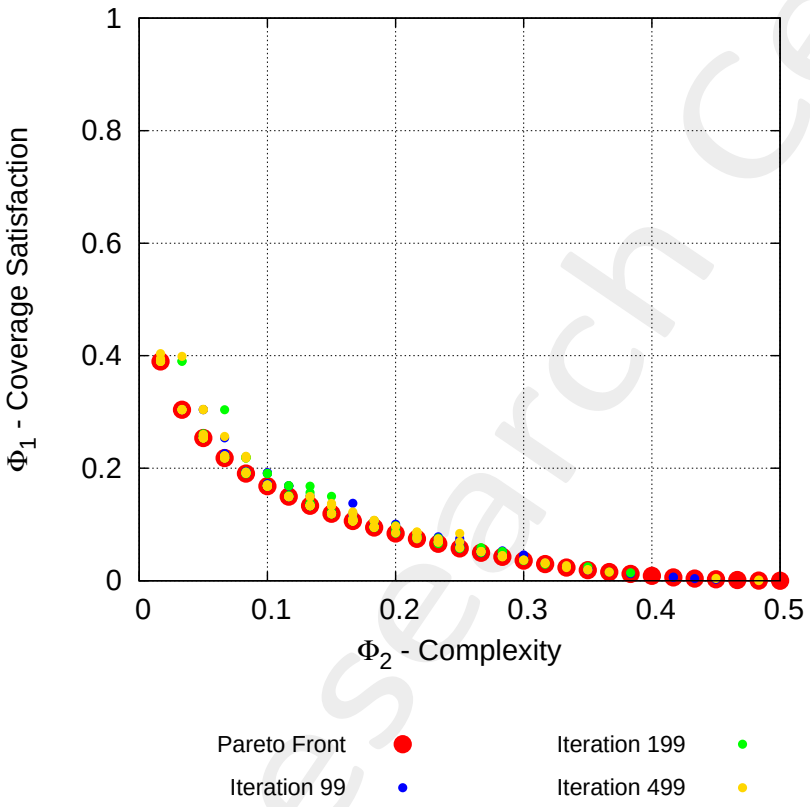

Figure 17: Optimization results (Pareto front in red)

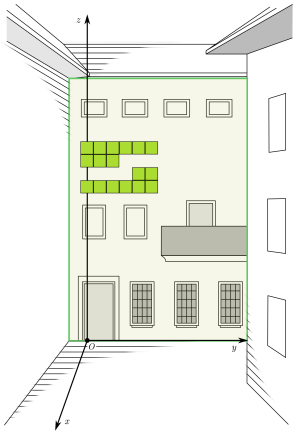

(*a*) Smart skin configuration

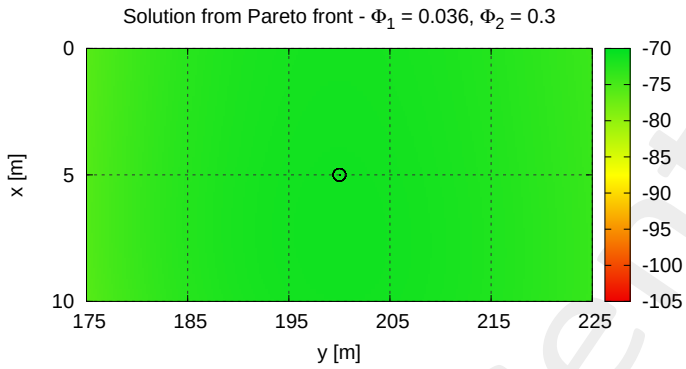

(*b*) Field inside the AoI

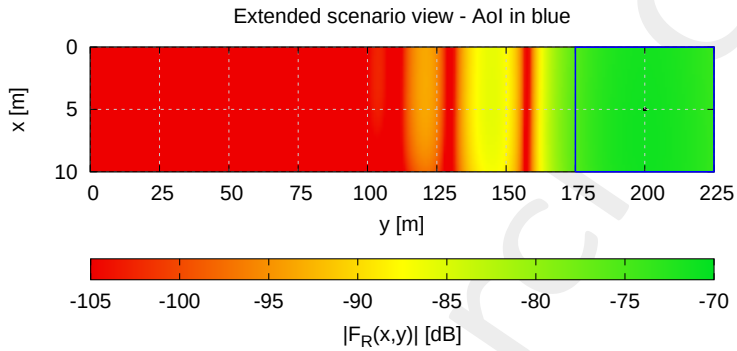

(*c*) Extended scenario view - AoI in blue

Figure 18: Solution ID 6383 - $\Phi_1 = 0.036$, $\Phi_2 = 0.3$

1.4.2 Distributed smart skin radiation

The distributed radiation condition in this final test case simply considers that each point is used as radiation direction by two metasurfaces, so the case with $N = 60$ metasurfaces has the same set of radiation points as the case for $N = 30$, but each of them is pointed at by two separate metasurfaces. The coordinates of these points and the respective metasurfaces are reported in Table VII, while the results are reported in Figures 19 and 20.

Table VII: Radiation points (x, y) coordinates for the distributed radiation of the smart skin for N = 60 metasurfaces

Surface ID	**x [m]**	**y [m]**	**Surface ID**	**x [m]**	**y [m]**	**Surface ID**	**x [m]**	**y [m]**
1, 31	2	182	**11, 41**	5	182	**21, 51**	8	182
2, 32	2	186	**12, 42**	5	186	**22, 52**	8	186
3, 33	2	190	**13, 43**	5	190	**23, 53**	8	190
4, 34	2	194	**14, 44**	5	194	**24, 54**	8	194
5, 35	2	198	**15, 45**	5	198	**25, 55**	8	198
6, 36	2	202	**16, 46**	5	202	**26, 56**	8	202
7, 37	2	206	**17, 47**	5	206	**27, 57**	8	206
8, 38	2	210	**18, 48**	5	210	**28, 58**	8	210
9, 39	2	214	**19, 49**	5	214	**29, 59**	8	214
10, 40	2	218	**20, 50**	5	218	**30, 60**	8	218

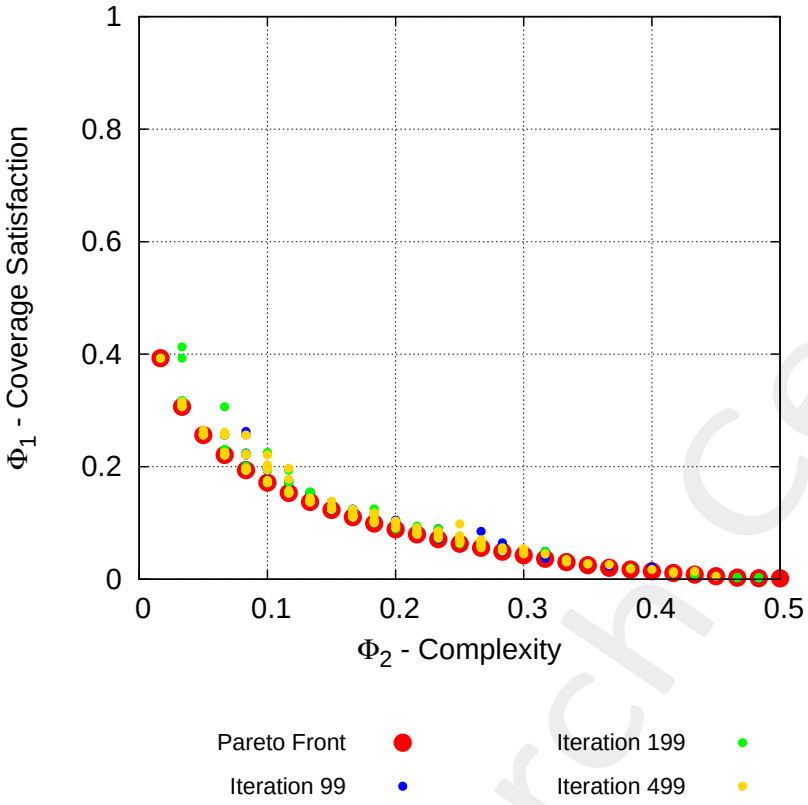

Figure 19: Optimization results (Pareto front in red)

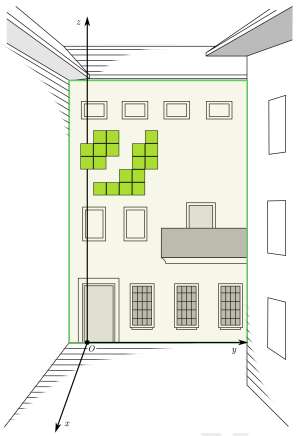

(*a*) Smart skin configuration

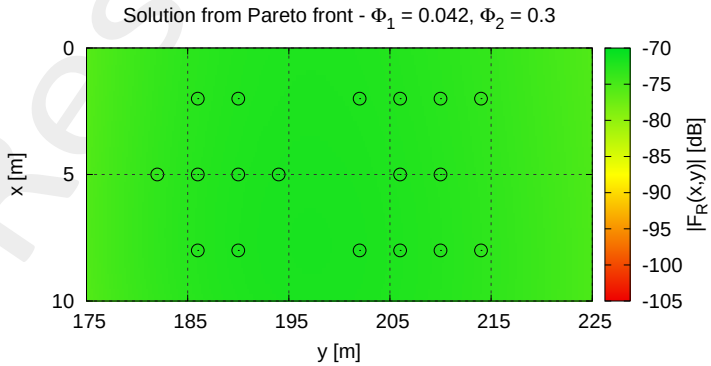

(*b*) Field inside the AoI

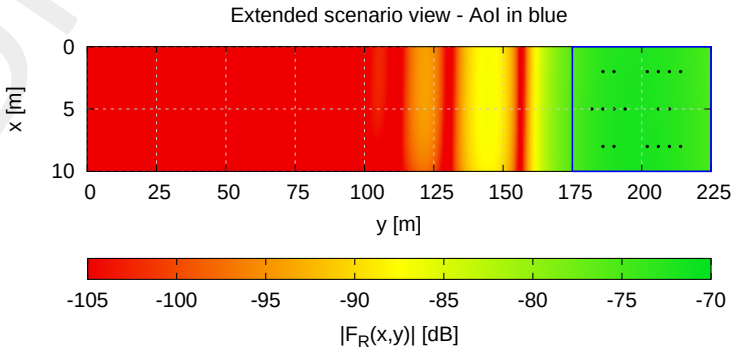

(*c*) Extended scenario view - AoI in blue

Figure 20: Solution ID 6668 - $\Phi_1 = 0.042$, $\Phi_2 = 0.3$

1.4.3 Considerations and comments

Comparing the data for this last set of optimizations, it is interesting to notice how the two obtained Pareto fronts perfectly correspond with one another. This behaviour can be justified with the vastly increased degrees of freedom of the optimization software (as it leads to the largest population for the genetic algorithm) and with a general increase in the maximum total field power achievable by the smart skin.

This increase in the available power is also reflected in the already mentioned presence of values of 0 for the ϕ_1 cost function, that indicates that the deployment with N = 60 metasurfaces is the only one in which the value of the field for all the considered observers exceedes the threshold value of -70 [dB], meaning that it offers an excellent coverage of the whole AoI.

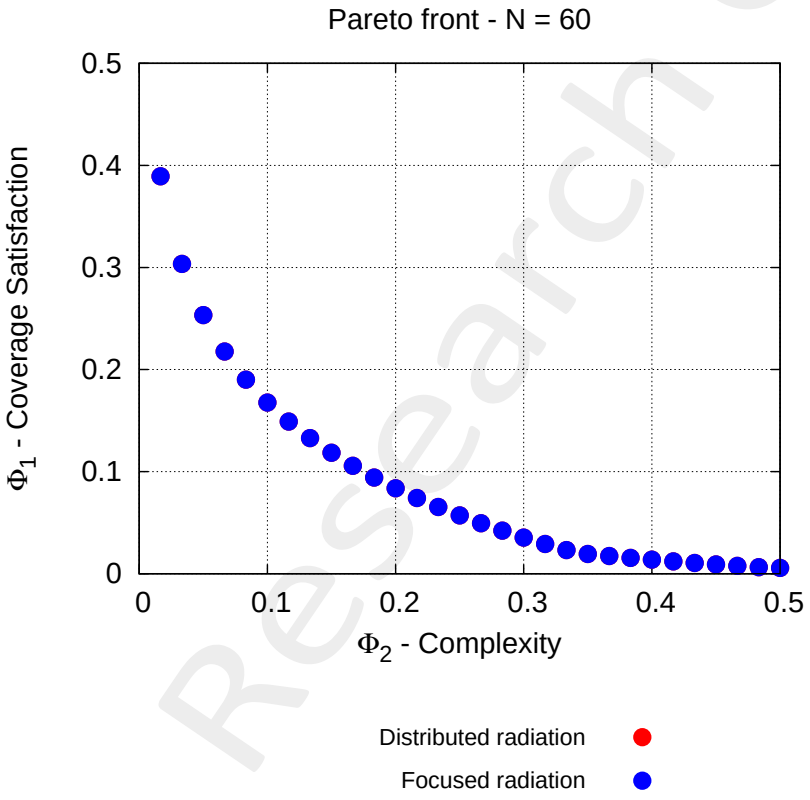

Figure 21: Comparison of focused and distributed radiation results fo N = 60

2 Conclusions

The presented activity aims at analyzing the feasibility and behaviour of an electromagnetic smart skin in a urban scenario, with an innovative approach given by the pairing of the analytical formulation with an evolutionary algorithm for the optimization of the problem.

2.1 Collocation in the State of the Art

To provide a sense of the current state of the art in the literature for what concerns reconfigurable metasurfaces, a thorough analysis has been proposed in the initial chapters of this document. As the presented activity lies its roots in a recently published paper on the topic of analytical formulation for EM fields, it can surely be considered as a further development of an already state-of-the-art contribution. In particular, the mathematical formulation has been deeply analyzed, and a software implementation has been derived from it, validating it against the results of the original author and using it as a basis for the development of all the produced additional software. In fact, starting from the analytical formulation of the electric field contribution of a surface, during the course of the activity a main software was developed for the simulation of a smart environment based on passive reconfigurable metasurfaces deployed so to form an EM smart skin, together with accessory statistical and graphical tools to help understand and visualize the results. Finally, the software was paired with an optimizer, where, through the use of a multi objective genetic algorithm a set of "optimal trade-offs" was computed, both for elementary scenarios and for more complex and realistic ones.

2.2 Current Limits and Future Developments

The activity as presented in the chapters above still offers some development options, and some issues are still open to future studies and solutions.

In the core software for the computation of the electric field, additions could be implemented to consider different signal polarizations for the impinging wave and for the radiated one, which would open the possibility for a study on polarization changes and polarization efficiency inside the smart environment. For what concerns the smart environment optimization, software-wise there are multiple degrees of freedom left to explore and optimize, e.g. the direction in which each metasurface radiates, the phase contribution of each of the surfaces or the effects of their grouping or tiling. Optimization-wise, there is still a certain degree of fine-tuning that can be performed on the NSGA-II algorithm, in order to obtain more representative solutions or examine further the ones already obtained, while the possibility remains for considering different parameters or cost function definitions for the definition of the optimization problem itself.

More information on the topics of this document can be found in the following list of references.

References

[1] Benoni, F. Capra, M. Salucci, and A. Massa, "Towards real-world indoor smart electromagnetic environments - A large-scale experimental demonstration," *IEEE Trans. Antennas Propag.*, vol. 71, no, 11, pp. 8450-8463, Nov. 2023 (DOI: 10.1109/TAP.2023.3305053).

[2] G. Oliveri, M. Salucci, and A. Massa, "Features and potentialities of static passive EM skins for NLOS specular wireless links," *IEEE Trans. Antennas Propag.*, vol. 71, no. 10, pp. 8048-8060, Oct. 2023 (DOI: 10.1109/TAP.2023.3301654).

[3] G. Oliveri, M. Salucci, and A. Massa, "Generalized analysis and unified design of EM skins," *IEEE Trans. Antennas Propag.*, vol. 71, no. 8, pp. 6579-6592, Aug. 2023 (DOI: 10.1109/TAP.2023.3281073).

[4] M. Salucci and A. Massa, "Unconventional sources for smart EM environments: An inverse scattering vision," *Reviews of Electromagnetics*, Invited Paper, vol 1, pp. 17-18, 2022 (DOI: 10.1109/MOCAST52088.2021.9493390).

[5] M. Salucci, A. Benoni, G. Oliveri, P. Rocca, B. Li, and A. Massa, "A multihop strategy for the planning of EM skins in a smart electromagnetic environment," *IEEE Trans. Antennas Propag.*, vol. 71, no. 3, pp. 2758-2767, Mar. 2023 (DOI: 10.1109/TAP.2022.3233714).

[6] G. Oliveri, F. Zardi, P. Rocca, M. Salucci, and A. Massa, "Constrained-design of passive static EM skins," *IEEE Trans. Antennas Propag.*, vol. 71, no. 2, pp. 1528-1538, Feb. 2023 (DOI: 10.1109/TAP.2022.3225593).

[7] G. Oliveri, P. Rocca, M. Salucci, D. Erricolo, and A. Massa, "Multi-scale single-bit RP-EMS synthesis for advanced propagation manipulation through system-by-design," *IEEE Trans. Antennas Propag.*, vol. 70, no. 10, pp. 8809-8824, Oct. 2022 (DOI: 10.1109/TAP.2022.3201700).

[8] A. Benoni, M. Salucci, G. Oliveri, P. Rocca, B. Li, and A. Massa, "Planning of EM skins for improved quality-of-service in urban areas," *IEEE Trans. Antennas Propag. - Special Issue on 'Smart Electromagnetic Environment'*, vol. 70, no. 10, pp. 8849-8862, Oct. 2022 (DOI: 10.1109/TAP.2022.3177284).

[9] G. Oliveri, F. Zardi, P. Rocca, M. Salucci, and A. Massa, "Building a smart EM environment - AI-Enhanced aperiodic micro-scale design of passive EM skins," *IEEE Trans. Antennas Propag. - Special Issue on 'Smart Electromagnetic Environment*,' vol. 70, no. 10, pp. 8757-8770, Oct. 2022 (DOI: 10.1109/TAP.2022.3151354).

[10] P. Rocca, P. Da RÙ, N. Anselmi, M. Salucci, G. Oliveri, D. Erricolo, and A. Massa, "On the design of modular reflecting EM skins for enhanced urban wireless coverage," *IEEE Trans. Antennas Propag. - Special Issue on 'Smart Electromagnetic Environment*,' vol. 70, no. 10, pp. 8771-8784, Oct. 2022 (DOI: 10.1109/TAP.2022.3146870).

[11] G. Oliveri, P. Rocca, M. Salucci, and A. Massa, "Holographic smart EM skins for advanced beam power shaping in next generation wireless environments," *IEEE J. Multiscale Multiphys. Comput. Tech.*, vol. 6, pp. 171-182, Oct. 2021 (DOI: 10.1109/JMMCT.2021.3121300).

[12] A. Massa, A. Benoni, P. Da RÙ, S. K. Goudos, B. Li, G. Oliveri, A. Polo, P. Rocca, and M. Salucci, "Designing smart electromagnetic environments for next-generation wireless communications," *Telecom*, Invited Paper, vol. 2, pp. 213-221, 2021 (DOI: 10.3390/telecom2020014).